Meas. Sci. Technol. 5 (1994) 1115–1123. Printed in the UK

A simple, high-performance Thomson-scattering diagnostic for high-temperature plasma research

D J Den Hartog and M Cekić

University of Wisconsin-Madison, Department of Physics, 1150 University Avenue, Madison, WI 53706, USA

Received 28 February 1994, in final form 6 June 1994, accepted for publication 14 June 1994

Abstract. This Thomson-scattering diagnostic is used to measure the electron temperature and density of the plasma in the Madison Symmetric Torus reversed-field pinch, a magnetic confinement fusion research device. This diagnostic system is unique for its type in that it combines high performance with simple design and low-cost components. In the design of this instrument, careful attention was given to suppression of stray laser line light with simple and effective beam dumps, viewing dumps, apertures and a holographic edge filter. This allows use of a single-grating monochromator for dispersion of the Thomson scattered spectrum onto the microchannel plate detector. Alignment and calibration procedures for the laser beam delivery system, the scattered light collection system, and the spectrometer and detector are described. A sample Thomson-scattered spectrum illustrates typical data.

1. Introduction

The Thomson-scattering diagnostic described in this paper is used to measure the temperature (T_e) and density (n_e) of the electrons in the high-temperature plasma produced in the Madison Symmetric Torus (MST) reversed-field pinch [1], a magnetic confinement fusion research device. A Thomson-scattering diagnostic is simple in concept and widely used [2, 3], but the difficulty in application arises because the cross section for Thomson scattering is very small. A further complication of the MST device is the fact that only a small aperture in the vacuum vessel is available for collection of Thomson-scattered photons. This combination of small collection étendue and low electron density made the implementation of a Thomson-scattering diagnostic for the MST device a difficult technical challenge. In practice, a typical shot of this diagnostic results in recording about 10^2–10^3 Thomson-scattered photons out of the 10^{19} fired into the plasma by the Q-switched ruby laser. Successful operation of this system meant implementing the complementary goals of suppressing collection of stray laser light and maximizing collection of Thomson-scattered photons. We have accomplished this on a limited budget by combining carefully designed low-cost optical and dispersive systems with carefully applied sophisticated optical elements such as a holographic edge filter.

A short introduction to the physics on which a Thomson scattering diagnostic is based will provide helpful background. In this application, the process of Thomson scattering refers to scattering of laser-produced monochromatic photons by free electrons in a plasma. When a photon is Thomson-scattered, the wavelength of the photon is Doppler-shifted by an amount proportional to the velocity of the electron. A Maxwellian distribution of electron velocities (usually a valid assumption in fusion research devices) yields a Gaussian distribution of scattered photon wavelengths. In the MST device, this Gaussian distribution is centred on the laser wavelength because the non-relativistic electrons have no directed radial velocity (the average velocity of the Maxwellian distribution is zero). The density and temperature of the electrons are then, respectively, proportional to the area and width squared of the Gaussian distribution. For the specific example of our Thomson-scattering diagnostic, a pulsed ruby laser is fired into the plasma and the scattered photons are counted in five channels, each collecting over a particular wavelength band. A data analysis procedure is then used to find the parent Gaussian distribution that is most likely to have given rise to the measured set of counts. Typical parameters for the MST device are $T_e = 200$ eV and $n_e = 1 \times 10^{19}$ m^{-3}.

2. Apparatus

Our Thomson-scattering diagnostic was not developed in isolation. We have tried to learn from others who

0957-0233/94/091115+09$19.50

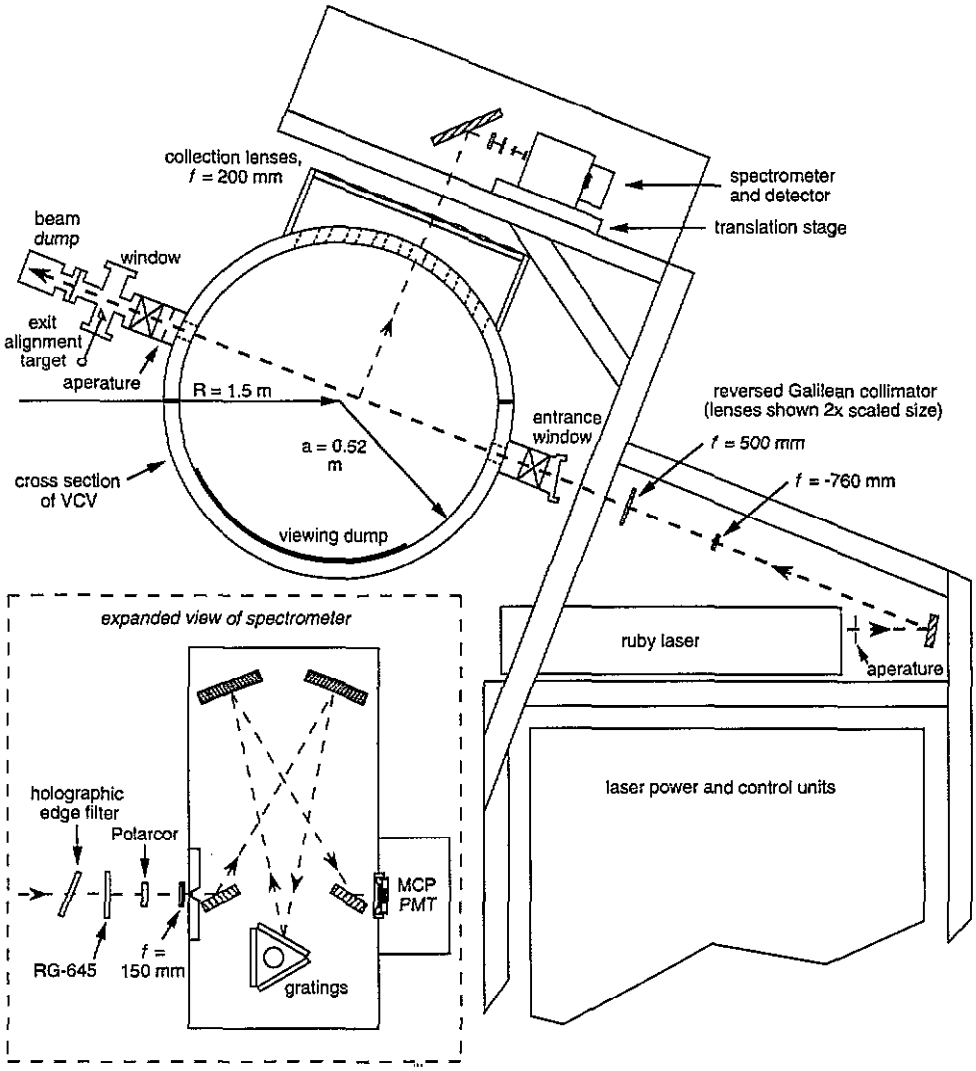

Figure 1. A side view of the Thomson scattering system on the MST device. Lenses are not shown to scale.

have built such systems. At the same time, we have implemented some unique features (described in this section), which maximize the overall performance of our system without adding undue complexity or cost. The following description of apparatus is organized such that light is followed through the optical train, beginning with the laser, through the scattered light collection, and into the spectrometer and detector. Refer to figure 1 for an overview of the system.

2.1. Thomson-scattering system hardware

2.1.1. The laser cart and detector platform. Most of the Thomson scattering equipment is mounted on a specially constructed portable aluminium cart. Notice that the cart and detector platform are a single mechanical structure; the laser system and detection system are coupled by this rigid structure. Neither the cart nor the detector platforms are directly coupled to the vacuum vessel. The cart is rolled up to the side of the vacuum vessel and fixed in place with levelling jacks mounted on neoprene damping pads. This aspect of portability and adaptability has proved to be important as the MST device has evolved.

The laser and most of the laser beam input optics are mounted on the top shelf of the cart. The lower shelves and floor of the cart hold the laser power supply, cooling system and control unit. Both cart and detector platform are covered by sets of easily removable and light-tight aluminium panels. These panels enhance the safety of personnel working in the range of a high-power laser and they lower the amount of radio-frequency noise reaching the detector electronics.

2.1.2. The laser and focusing optics. The Q-switched ruby laser system was manufactured by JK Lasers (now Lumonics). The rods are linear flash-lamp-pumped, a configuration that we have found to be reliable and easy to maintain. The system contains as oscillator rod and one amplifier rod; the beam is multimode because it is not spatially filtered. Q-switching is done with a Pockels cell. The straight-through configuration of the laser head allowed a He–Ne alignment laser to be mounted such that its beam enters the optical train behind the rear

Table 1. Parameters of the ruby laser.

Wavelength	694.3 nm
Maximum output energy	10 J
Output beam diameter	16 mm
Pulse duration (FWHM)	40 ns
Polarization	Horizontal
Beam divergence	90% within 1.2 mrad

mirror of the ruby laser, thus ensuring coincidence with the ruby laser beam. The parameters of the ruby laser are listed in table 1.

As can be seen in figure 1, the ruby laser beam enters the vacuum vessel 22° below the horizontal midplane of the toroid. Most data on the MST device are taken with the laser beam focused such that the waist (the point from which scattered light is collected) is at the estimated position of the plasma current axis. Occasionally we have taken data at other radial positions [4].

After exiting the laser, the laser beam passes through a 16 mm diameter aperture. This aperture removes stray and rapidly diverging light that might otherwise inadvertently reflect into the collection optics. The beam is then folded back into the reversed Galilean collimator by a kinematically mounted mirror. The collimator produces a scattering volume that is matched onto the entrance slit of the spectrometer by the collection optics. The collimator lenses are mounted such that the plane of each lens is slightly off perpendicular to the optical axis. This prevents potentially damaging back reflection of the beam into the laser. The position of each lens is x, y and z adjustable.

The laser beam, once through the collimator, passes into the vacuum vessel through an input window. The input window is mounted on a valve and is 10° off perpendicular to the laser beam. All of the optical elements in the laser beam delivery system are UV grade fused silica and 'V-line' anti-reflection-coated to minimize reflection at the ruby laser wavelength. The optical surfaces are checked for dust daily and are cleaned with a puff from an air bulb. In addition, HEPA (high efficiency particulate absolute) filtered air flows into the laser and beam optics enclosure, which is kept at a slight positive pressure in order to prevent dust migration into it.

2.1.3. Beam dumping and stray light reduction. Only a small fraction of the photons in the laser beam are Thomson-scattered into the collection optics. The rest of the photons must be dumped or they will overwhelm the rejection of the spectrometer and bury the Thomson-scattered signal.

The most important element of the stray-light-reduction system is the laser beam dump, shown in figure 2. This dump is an evolutionary improvement of the dump installed on the TNT-A tokamak [5]. The ruby laser beam coming into the dump is horizontally polarized. It is incident upon the first set of absorptive blue and green filter glasses at Brewster's angle. The small reflected beam is absorbed by the second piece

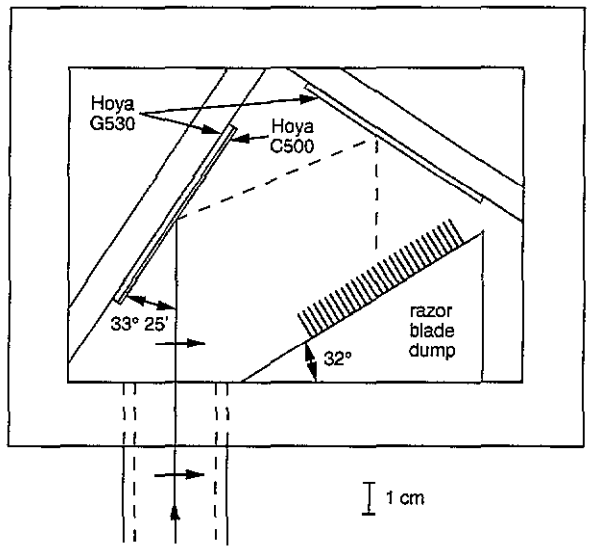

Figure 2. The ruby laser beam dump. The arrows perpendicular to the laser beam indicate horizontal polarization.

of filter glass and the razor blade dump. This design is extremely compact and robust, having survived thousands of high-power shots without visible damage.

As the laser beam exits the vacuum vessel it passes through an aperture beam dump (figure 1) that picks off the widely diverging rays of the beam that are created by imperfections in the input optics. This dump consists of an annular opening through which the laser beam passes. The annulus is surrounded by closely spaced V-grooves cut into the aluminium substrate. The peaks of the grooves are sharp edges separated by about 1.6 mm; the depth between the grooves is 3.2 mm. The exposed aluminium surfaces of this dump and the main beam dump are coated with a layer of black graphite dust applied in an isopropyl alcohol suspension.

The other important stray-light-reduction component is the viewing dump mounted opposite the collection lens in the vacuum vessel. The overwhelming majority source of stray light is simply laser line light that has diverged from the main beam path and ends up being reflected around inside the vacuum vessel. However, most of the stray light enters the collection optics by reflecting into the collection solid angle off the wall exactly opposite the collection port. The viewing dump covers this area and absorbs most of the light incident upon it. The viewing dump itself is simply a set of commercial integrated circuit cooling blocks mounted on the wall of the vacuum vessel. The blocks are black anodized aluminium and consist of 4 mm high vertical fins spaced 3 mm apart. This novel viewing dump is close enough to the wall for it not to interact with the plasma, yet is cheap and fairly efficient.

2.1.4. Collection optics. The system of collection optics is shown in figure 1. The biconvex collection lens has a focal length of 200 mm and is mounted in a flange, which is bolted to the box-port on the MST device. It is BK-7 glass and is anti-reflection-coated (as are all optical elements in the collection

system). The lens forms the vacuum seal and is exposed to the scattering volume through a 50 mm diameter hole in the vacuum vessel. (This is the aperture that limits the étendue of the collection optics to a rather small 0.19 mm^2 sr.) The collection lens focuses the approximately 1.0 mm×32 mm cylindrical scattering volume onto the 0.5 mm×16 mm entrance slit of the spectrometer. The light rays are matched onto the collimating mirror of the spectrometer by a field lens mounted just in front of the entrance slit. This field lens is a cylindrical lens of 150 mm focal length; the axis of the lens is perpendicular to the entrance slit.

As shown in figure 1, eight collection lenses are mounted in the box-port flange. These look through eight 50 mm holes in the vacuum vessel and may be used to obtain radial profiles of electron temperature and density. With the presently available equipment, such scans have to be done position-by-position. This requires full re-alignment of the optics at each position and is very tedious.

There are some other important elements in the collection system. The polarizer is a Corning Polarcor, which has better transmission above 700 nm than the typical plastic dichroic sheet. It transmits the horizontally polarized Thomson-scattered light and blocks half the randomly polarized plasma background light (which in the MST device is mostly bremsstrahlung radiation and is usually a small fraction of the Thomson-scattered signal). The Schott RG-645 colour filter passes wavelengths longer than 690 nm; only the long-wavelength side of the Thomson-scattered spectrum is recorded. The short-wavelength side of the spectrum is rejected because it contains the hydrogen α line at 656 nm.

In addition to the colour glass filter, which has a slowly changing transmission function, we have installed a holographic edge filter to reject the ruby laser line. These filters were developed initially by Physical Optics Corporation for use in Raman spectroscopy, an application that (like Thomson scattering) requires separation of laser line light from spectral features wavelength shifted only a few nanometres from the laser line. Our filter, as manufactured for perpendicularly incident light, features a blocking optical density (OD) of 5 or better at $\leqslant$ 698 nm and a narrow transition region leading to $\geqslant$ 70% transmission at $\geqslant$ 709 nm. We tilt this filter to move the transition region closer to the ruby laser wavelength of 694 nm. This filter in combination with our single-grating spectrometer provides sufficient rejection of the ruby laser line wavelength that no such 'background' photons are counted by the detector during normal operation of the diagnostic. Such an achievement normally requires rejection by an expensive double- or triple-grating spectrometer.

2.1.5. Alignment of the optical system. The key to a functional Thomson scattering diagnostic is successful alignment of the beam and collection optical systems. An overview of the procedure we use follows.

(i) Adjust the He–Ne laser such that its beam spot coincides with the mark made by the ruby laser on a piece of burn paper (such as that made by Kentek).

(ii) Insert the exit alignment target (figure 1). This is a small block of aluminium cut at 45° to the laser beam. The beam optics can now be adjusted to bring the beam through the vacuum vessel and into the beam dump.

(iii) Now the collection optics may be aligned. The alignment target that is inserted is not shown in figure 1, since it is normally retracted to a position just to the side of the laser entrance window. The target is mounted on a rod that, when inserted into the vacuum vessel, travels nearly parallel to the path of the ruby laser beam. The face of the target is 45° off perpendicular to both the laser beam axis and the collection optics axis. Adjust the collection optics such that the alignment laser spot is imaged onto the entrance slit of the spectrometer. Final adjustments can be made by firing the ruby laser into a plasma and maximizing the Thomson-scattered signal that is collected.

Our Thomson-scattering system has proven to be mechanically stable and will remain aligned for periods of about a month.

2.1.6. The spectrometer and detector. The spectrometer (figure 1) is a modified Jarrell-Ash MonoSpec 27 monochromator. It is of cross Czerny–Turner design and 275 mm focal length. The throughput is effectively $f/4.4$ in the wavelength range of the Thomson-scattered light. This matches the $f/4.4$ of the optical collection system. This spectrometer has a triple-grating turret, which allows quick grating changes. A classically ruled grating (1200 grooves per millimetre) with a blaze wavelength of 500 nm is most often used on the MST device; it provides dispersion appropriate to measure electron temperatures in the range 50–500 eV. The other two gratings are of 600 and 1800 grooves per millimetre for higher and lower temperatures.

The detector at the exit plane of the spectrometer is an ITT F4149 microchannel plate (MCP) photomultiplier tube (PMT) with a multi-alkali photocathode and a 10 × 10 pin anode array. (The Thomson-scattering system on the Torus II tokamak used this same detector [6].) The photocathode of the MCP PMT is coincident with the exit plane of the spectrometer. (The perimeter of the photocathode window is carefully masked with a flat black aperture to increase rejection of the ruby laser line.) Photoelectrons from the photocathode cascade down the microchannel plates (this is where the electron gain occurs) and are collected at the output anode array. (We have examined this process in detail in the context of its impact upon the uncertainties in the derived quantities [7].) The 10 × 10 anode array on the MCP PMT is wired such that it consists of one vertical row of ten anode pins, three vertical rows of 20 anode pins each, and one vertical row of 30 anode pins. The Thomson-scattered spectrum is recorded by these five bands of pins (each band is a wavelength channel). The narrow channel (one row of pins) is closest to the laser line, the wide channel (three rows of pins) is furthest

from the laser line. Computer simulations of various band configurations [8] suggested that the one chosen leads to the most robust reconstruction of the Gaussian-shaped scattered spectrum. Each channel collects a roughly equivalent number of photons, ensuring that each section of the spectrum is well defined. The measured instrument function of the spectrometer and a sample Thomson-scattered spectrum will be shown and discussed in sections 2.2 and 2.4.

The MCP PMT is mounted in a brass electrostatic shield, which is electrically isolated from the spectrometer. The MCP PMT is powered by a gateable power supply similar to the one used in the Thomson-scattering system on the Tara random mirror [9]. This power supply performs a number of functions. It provides the high voltage for the MCP assembly. This high voltage is continuously switched on while the diagnostic is in operation. The photocathode is normally biased 33 V positive with respect to the entrance of the microchannel plates; this rejects light from the plasma that would saturate the MCP. The MCP PMT is gated on by swinging the photocathode 133 V negative with respect to the entrance of the MCP. The gateable power supply does this in less than 100 ns, although the MCP PMT requires a few microseconds to stabilize after being gated on. Finally, the power supply also provides the necessary 100 V between the exit of the microchannel plates and anode pins. The anode pins are at a virtual earth through 50 Ω.

2.1.7. The data acquisition system. The equipment and interconnections in the data acquisition system are shown in figure 3. This is a complex system; a timeline detailing the progression of pulses and data through the system is shown in figure 4. The explanation below will follow this same chronological progression.

The main timing panel module provides the initial trigger pulse. This module is part of the sequence of pulsers that control all MST operations. The module delivers a pulse to the laser 1.25 ms before the laser actually fires. During this time interval the flash lamps pump the ruby rods. When the rods have reached a population inversion, the internal timing circuitry of the laser produces a pulse that opens the Pockels cell. This produces a Q-switched 40 ns FWHM pulse of light, which proceeds to travel through the optical train. The laser timing circuitry also produces a Pockels cell 'sync' pulse with a leading edge about 4.9 μs before the laser light pulse. This leading edge triggers the MCP PMT gate section of the Thomson-scattering 'timing box'. After a delay of 2.8 μs, this box produces a 2.5 μs MCP PMT photocathode gate pulse. This gate pulse travels to the MCP gateable power supply which gates the MCP PMT on as described in the previous section. The gain of the MCP PMT is stable about 2 μs after it is gated on.

The above sequence of gate pulses happens on a relatively slow time scale. A much faster timing sequence is required to control the LeCroy 2250L digitizer that records both the Thomson-scattering data and the plasma background light. This sequence begins

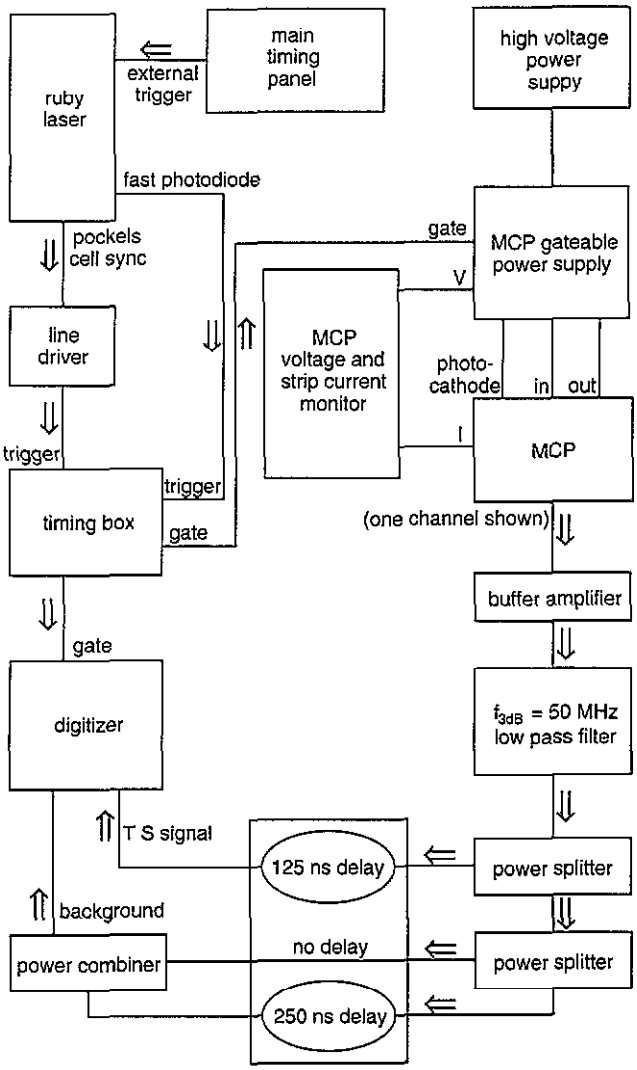

Figure 3. The data acquisition system.

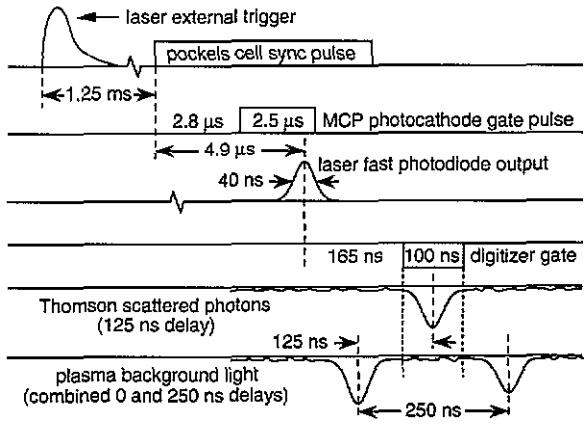

Figure 4. The sequence of events during a data acquisition shot.

at the fast photodiode output of the ruby laser. The laser optical train contains a picosecond rise-time photodiode that follows the shape of the laser light pulse. The photodiode pulse triggers the digitizer gate section of the Thomson-scattering timing box. This produces a 100 ns wide digitizer gate that begins before the pulse of Thomson-scattered data reaches the digitizer. Initial synchronization of these events was done empirically by

cutting RG-58 coaxial cable to a length that provided the appropriate delay.

The data from a spectrometer wavelength channel reach the digitizer in the following manner. The Thomson-scattered photons that reach the MCP PMT produce a pulse of current, which follows the time-shape of the laser pulse. This current pulse flows into the 50 Ω input of an amplifier. The amplifier drives the pulse through about 9 m of coaxial cable to a 50 MHz low-pass filter on the input of the time-delay box. This filter removes the 80 MHz Pockels cell switching noise that the MCP PMT picks up. (An MCP PMT is a very effective noise antenna.) For the moment, ignore the delay lines. The current pulse moves from the filter to the digitizer, which integrates the current pulse and produces a number of counts proportional to the amount of charge that has flowed into its input. The gain of the MCP PMT and amplifiers has been adjusted so that one photon is approximately two thirds of a digitizer count [7].

Return to the delay lines that follows the 50 MHz filter. The 125 ns delay line is a coil of 25 m of RG-58 coaxial cable, the 250 ns delay is twice that length. The actual Thomson-scattered signal passes through the 125 ns delay. The plasma background light that precedes and follows the pulse of Thomson-scattered photons passes through the 250 ns delay and no delay respectively. This allows the average of the plasma background light before and after the Thomson-scattered signal to be digitized concurrently with the Thomson-scattered signal. The signal remaining after subtraction is the Thomson-scattered light. Reduction of the raw Thomson-scattering data for the derived quantities T_e and n_e and their uncertainties has been described elsewhere [7].

2.1.8. Sawtooth synchronization. One of the most interesting phenomena in MST device plasmas is the sudden burst of dynamo activity similar to sawtooth events in tokamaks. The period of these dynamo events is typically 2 ms and each event is similar. Measurement of the variation of T_e and n_e over the period of the sawtooth event is crucial for elucidation of the physical mechanism that governs these events. In order to perform this measurement with our single-shot Thomson-scattering diagnostic, we developed a trigger and timing circuit, which allowed precise control of laser firing time in relation to the phase of a dynamic event. A series of nominally identical plasma discharges is then all that is needed to map out the variation of T_e and n_e.

In normal operation, the laser firing time is controlled by the main timing panel (figure 3), which fires the laser at a pre-set time during the plasma discharge. Feedback control of the firing time is done by linking it to the sawtooth modulations of the current in the MST device's toroidal field windings. In this mode of operation the laser trigger originates in the pulse-shaping and delay network (figure 5) coupled by a Rogowski coil to the current in the toroidal field windings. The integrator gate is pre-set to block the rapidly varying signal during

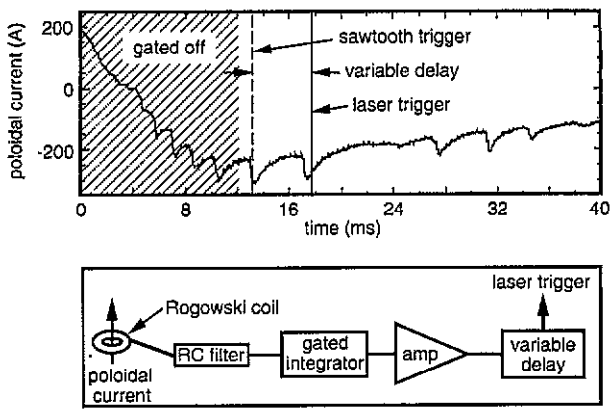

Figure 5. The laser trigger circuit for sawtooth synchronization.

the plasma formation phase. The time constants of the *RC* filter and the integrator are chosen such that the intermediate frequency and amplitude sawtooth events are separated from the high-frequency, low-amplitude noise. The actual laser firing time (and thus the phase of the dynamo event at which data is taken) is set by the variable delay unit.

2.2. Spectrometer calibration

Accurate Thomson-scattering measurements require a calibrated spectrometer. Basic calibration includes measurement of the centre and width of the wavelength channels and relative (channel-to-channel) sensitivity. In the following section we describe a self-consistent set of calibration and data reduction procedures, which have markedly evolved since we began operation of this diagnostic over five years ago.

2.2.1. The instrument function. For our Thomson-scattering application, one of the most important characteristics of the spectrometer–detector system is the instrument function, which we define as the response (in digitizer counts) of each of five detector channels versus the wavelength (in nanometres) of the incident monochromatic light. The instrument function is characterized by the central wavelength λ_c and the full-width at half-maximum (FWHM) $\Delta\lambda_{1/2}$ of each channel.

Calibration should be done under conditions as similar as possible to those of the actual experiment. Therefore, we measure the instrument function using a special LED pulser, which approximates the intensity and pulse shape of the plasma-scattered laser light. A narrow 1.3 nm band, centred at 708.0 nm, is cut by an interference filter out of a 30 ns pulse of light produced by a column of Hewlett-Packard HEMT-6000 LEDs. This light is focused through the colour glass filter and the polarizer (figure 1) to fill the spectrometer entrance slit. The Raman edge filter is removed for this measurement and calibrated separately in a spectrophotometer. The LED pulser produces electronic synchronization pulses similar to those produced by the laser timing system described in section 2.1.7, thus ensuring compatibility with the data acquisition system.

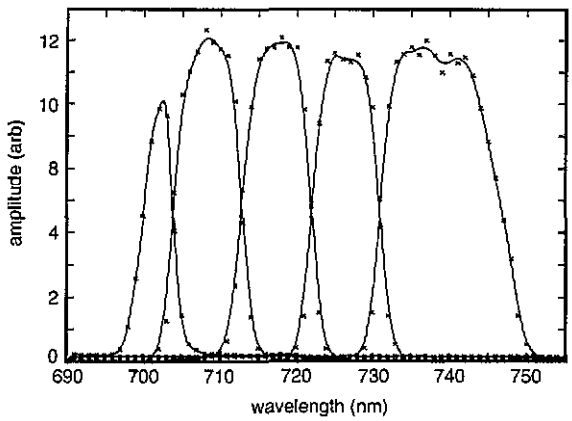

Figure 6. The instrument function of the spectrometer.

The instrument function shown in figure 6 was obtained by scanning the LED pulser light over the microchannel plate detector by rotating the spectrometer grating. The data points shown represent 64 30 ns light pulses. The wavelength scale shown in figure 6 has been adjusted to correspond to the set-up used during acquisition of actual Thomson-scattering data. The response curve of each individual channel is roughly trapezoidal. To a good approximation the width of each channel is equal to the FWHM of each trapezoid and the channel central wavelength is the centre of the trapezoid. The slight asymmetry in the shape of the channels (most obviously on channel 5 between 740 and 750 nm) is probably caused by minor misalignment between the exit focal plane and the photocathode of the MCP PMT. It is neglected in the above approximation, but explicitly accounted for in the absolute Raman calibration described below.

2.2.2. Detection efficiency. Measurement of the relative sensitivity of each detector channel is done with a calibrated quartz–halogen tungsten light source. This standard source is powered by a stable DC current supply and has a known spectral irradiance.

The efficiency of each detector channel i can be quantified in terms of conversion factors C_i defined by

$$P_i = C_i D_i \tag{1}$$

where P_i is the effective number of photoelectrons at the detector photocathode and D_i is the corresponding number of digitizer counts. Fortunately, it is not necessary to measure P_i directly. Instead, we use the fact that repeated measurements of the intensity of a stable light source will be distributed in a Poisson statistical distribution [7, 10]. Conversion factors C_i are then simply given by

$$C_i = D_i/(\sigma_{n-1})^2 \tag{2}$$

where σ_{n-1} is the standard deviation of a set of D_i measurements. Actual calibration is done by patiently recording a set of about 8000 D_i measurements, illuminating the spectrometer–detector system exactly as it is configured in plasma experiments.

2.3. Absolute electron density measurements

In addition to the procedures described above, measurement of the plasma electron number density necessitates absolute calibration of the transmission efficiency of the entire scattered light collection and detection apparatus. This calibration is much more demanding than the prerequisite spectrometer calibration (section 2.2) and is accomplished via a Raman-scattering procedure.

The electron number density n_e can be expressed in terms of the normalized 90° Thomson-scattering spectrum $S_T(\lambda_s)$ (the Gaussian fit of raw data) [2, 3, 11] by

$$n_e = \frac{\int_0^\infty S_T(\lambda_s)\,d\lambda_s}{N_I \sigma_T L \Delta\Omega\,\eta T} \tag{3}$$

where σ_T is the differential 90° Thomson-scattering cross section, N_I is the number of incident photons, L is the length of the scattering volume, $\Delta\Omega$ is the observation solid angle, η is the quantum efficiency of the detector and T is the transmission of the scattered-light collection and detection system.

All parameters in equation (3) can, in principle, be measured or calculated *ab initio*. In practice, this is difficult to do with the required accuracy. The solution is to measure T via comparison with a different scattering process in which the number density of scatterers is known. A fundamental requirement is that these scattering measurements be compatible with the laser and detection system as optimized for plasma measurements. Rayleigh scattering of laser light from a gas of known pressure, which is frequently utilized for absolute calibration [11–13], is an unacceptable choice for the MST Thomson diagnostic because the holographic edge filter suppresses the unshifted 693.4 nm ruby laser light.

In contrast, a calibration technique based on rotational Raman scattering [11, 14–16] is not limited by such a difficulty. When a photon is Raman-scattered, its wavelength is shifted by an amount proportional to the change in energy of the rotational or vibrational quantum state of the scattering molecule. By choosing an appropriate gas (N_2, H_2, D_2 or SF_6) as scattering medium one can achieve partial overlap of the wavelength ranges of Thomson and Raman scattering. Then, for a single channel i of the spectrometer, the Raman analogue of equation (3) is

$$n_{gas} = \frac{C_i S_{ri}}{N_i R_i K_i} \tag{4}$$

where n_{gas} is the number density of light-scattering gas molecules, C_i is the sensitivity constant, S_{ri} is the number of raw data counts, N_i is the number of incident photons (proportional to laser energy), R_i is a calculated factor [11, 17] corresponding to a scattering cross section and $K_i = L\Delta\Omega\,\eta T$ is a geometric calibration factor identical to the one in equation (3). In principle, calibration can be done in any wavelength channel. In practice, the small Raman-scattering cross section and small energy shift between rotational states usually favour the channel closest to the laser wavelength.

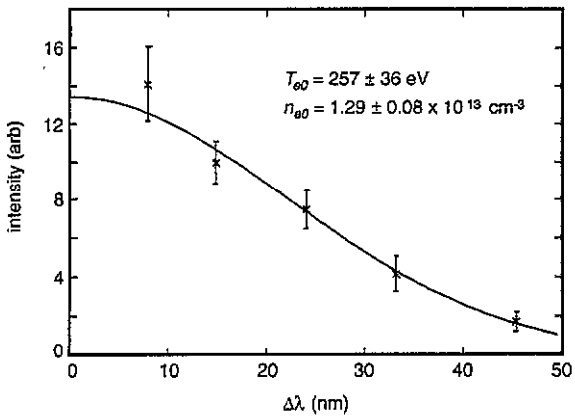

Figure 7. A spectrum from a typical shot of the MST Thomson-scattering diagnostic.

A problem arises during the above procedure because all molecular gases produce Rayleigh-scattered light. Its contribution is strongly reduced by the rejection of the spectrometer and holographic edge filter. However, because the Rayleigh-scattering cross section is approximately 10^4 times larger than the effective Raman cross section, leakage of Rayleigh-scattered light into the channel being used for Raman calibration has be taken into account. Ignoring this factor would lead a systematic error in electron density measurement of about 20% for the MST device's diagnostic.

The amount of Rayleigh-scattered light that 'leaks through' the rejection of the spectrometer can be easily measured by scattering laser light from a known density of a monatomic gas (which does not Raman-scatter light). About 10^4 Pa of argon works well; at higher pressures the gas may break down at the focus of the laser where the electric field is large. Knowledge of the Rayleigh cross sections of argon and the gas selected for the Raman calibration procedure allows the Rayleigh contribution to be subtracted from the counts recorded during Raman calibration.

2.4. A sample result

One example of MST Thomson-scattering data is shown in figure 7. The raw data shown have been scaled by relative channel sensitivity and the digitizer pedestal and plasma background light have been subtracted. The Gaussian fit to the data is shown as a full line (a description of the fitting algorithm that we have developed is given in [7]). These data are representative of a typical MST device discharge; the plasma current was 340 kA and the chord-average electron density was 0.85×10^{13} cm^{-3}. The central electron density of 1.29×10^{13} cm^{-3} is as expected from the parabolic density profile typically seen in the MST device. The central electron temperature is consistent with soft x-ray spectrum measurements taken with a Si(Li) detector.

3. Summary

The MST Thomson-scattering diagnostic is operated routinely to make single-point measurements of electron temperature and density. The system was designed to be relatively simple, reliable and of low-cost. These goals were achieved by paying careful attention to suppression of scattered laser line light, which in turn allows successful use of a single-grating spectrometer. The entire system is integrated into a compact rigid supporting structure, which is easily accessible for maintenance and alignment. Finally, this diagnostic is operated and maintained by one person, an important advantage in a small research group such as that on the MST device.

4. Future development

Preliminary design work is being done for a multi-point, multi-shot Thomson-scattering diagnostic capable of radially resolving high-frequency fluctuations in T_e and n_e. The heart of this system will be a multi-pulse Q-switched ruby laser capable of producing up to 20 1 J pulses, each pulse separated by 5–50 μs. The low-divergence laser beam will be multi-passed through the plasma for 20 or more passes in order to increase the number of Thomson-scattered photons [18]. The spectrometer that we plan to use was custom built for the Thomson-scattering system on the ZT-40M RFP. It is $f/2$ to match the fibre optic input and has very large étendue combined with good rejection of the ruby laser line. This system should provide the capability of measuring the radial evolution of T_e and n_e during a single sawtooth event to accuracies of within a few per cent.

Acknowledgments

Many people have contributed to the design, construction and operation of this diagnostic, including R Dexter, S Hokin, D Holly, K Melzacki, J Sarff, M Thomas and the helpful craftsmen of the University of Wisconsin Physics Department Student and Instrument Shops. This work is supported by the US Department of Energy.

References

[1] Dexter R N, Kerst D W, Lovell T W, Prager S C and Sprott J C 1991 The Madison Symmetric Torus *Fusion Technol.* **19** 131

[2] Sheffield J 1975 *Plasma Scattering of Electromagnetic Radiation* (New York: Academic) p 46

[3] Hutchinson I H 1987 *Principles of Plasma Diagnostics* (Cambridge: Cambridge University Press) p 239

[4] Cekić M, Den Hartog D J, Fiksel G, Hokin S A, Holly D J, Prager S C and Watts C 1992 Energy confinement studies and profile investigations of the MST plasmas *Bull. Am. Phys. Soc.* **37** 1607 (abstract only)

[5] Nagayama Y, Sakuma K and Toyama H 1982 Thomson scattering measurements in non-circular tokamak TNT-A *Japan. J. Appl. Phys.* **21** 1056

[6] Levinton F M and Navratil G A 1983 Multipoint Thomson scattering *Rev. Sci. Instrum.* **54** 35

[7] Den Hartog D J and Ruppert D E 1994 Photon counting spectroscopy with a microchannel plate detector *Rev. Sci. Instrum.* submitted
Den Hartog D J and Ruppert D E 1993 Photon counting spectroscopy as done with a Thomson scattering diagnostic *Report No DOE/ER/53198-230* University of Wisconsin, Madison, USA

[8] Den Hartog D J and Dexter R N 1987 Thomson scattering in the poloidal divertor RFP at Wisconsin *PLP 1023* University of Wisconsin—Madison Plasma Physics (unpublished report)

[9] Casey J A and Irby J H 1986 Thomson scattering in the Tara tandem mirror central cell *Rev. Sci. Instrum.* **57** 1804

[10] Hart G W, Levinton F M and McNeill D H 1986 Study of the effects of photoelectron statistics on Thomson scattering data *Rev. Sci. Instrum.* **57** 2218

[11] McCool S C 1982 Thomson scattering on the Pretext Tokamak *PhD Thesis* University of Texas at Austin
McCool S C, McCool I L, Bengtson R D and Phillips P E 1981 Calibration of Thomson scattering density measurements *FRCR 234* University of Texas at Austin Fusion Research Center (unpublished report)

[12] Rudder R R and Bach D R 1968 Rayleigh scattering of ruby-laser light by neutral gases *J. Opt. Soc. Am.* **58** 1260

[13] DeSilva A W and Goldenbaum G C 1970 *Methods of Experimental Physics* vol 9A, ed H R Griem and R H Lovberg (New York: Academic) p 61

[14] Röhr H 1977 Raman scattering—a possibility of calibrating laser scattering devices *Phys. Lett.* **60A** 185; 1981 Rotational Raman scattering of hydrogen and deuterium for calibrating Thomson scattering devices *Phys. Lett.* **81A** 451

[15] Howard J, James B W and Smith W I B 1979 Rotational Raman calibration of Thomson scattering *J. Phys. D: Appl. Phys.* **12** 1435

[16] Bogomolov G D and Letunov A A 1979 Amplitude calibration of system for laser plasma diagnostics by rotational Raman scattering in hydrogen and deuterium *Sov. J. Plasma Phys.* **5** 774

[17] Penney C M, St Peters R L and Lapp M 1974 Absolute rotational Raman cross section for N_2, O_2 and CO_2 *J. Opt. Soc. Am.* **64** 712

[18] Akatova T Yu, Bulyginsky D G, Goncharov S G, Gusev V K, Ilyin V S, Kantor M Yu, Razdobarin G T and Shilnikov A N 1985 The multipass Thomson scattering system for plasma diagnostics in the FT-1 tokamak *Preprint 956* Physical-Technical Institute of the Academy of Science of the USSR (Ioffe Institute) (abstract in English, text in Russian)